RESEARCH ARTICLE | SEPTEMBER 26 2023

Assessment of heated reverse Taylor cylinder experiments for the calibration of tantalum strength models

B. Thorington-Jones; G. Whiteman ✉; L. C. Smith; D. J. Chapman; D. E. Eakins

AIP Conf. Proc. 2844, 260012 (2023)
https://doi.org/10.1063/12.0020430

Assessment of Heated Reverse Taylor Cylinder Experiments for the Calibration of Tantalum Strength Models

B. Thorington-Jones[1], G. Whiteman[1, a)], L.C. Smith[2], D.J. Chapman[2], and D.E. Eakins[2]

[1]*AWE, Aldermaston, Reading, RG7 4PR. United Kingdom*
[2]*University of Oxford, Dept. of Engineering Science, Begbroke Science Park, Oxford, OX5 1PF. United Kingdom*

[a)]Corresponding author: glenn.whiteman@awe.co.uk

Abstract. A series of heated reverse Taylor impact experiments have been undertaken on pure polycrystalline tantalum to investigate the individual and interdependent effects of strain-rate and temperature. Impact velocities and initial temperatures in the ranges 112-185 m/s and 293-954 K were studied. Velocimetry and high-speed imaging were used to record time-resolved deformation of the rods. The data is compared to Lagrangian hydrocode simulations and the performance of three strength models (Steinberg-Guinan, Preston-Tonks-Wallace and the LMS13 multiscale model) are assessed. Overall, the LMS13 model was able to reproduce the deformed rod profile and the velocimetry most accurately.

INTRODUCTION

Traditional Taylor impact experiments consist of the impact of a right cylinder onto a rigid anvil. The test was originally devised to provide an estimation of dynamic material strength derived from measurements of the final deformed profile [1, 2]. As the sample is subjected to a wide range of stress, strain and strain-rates it is nowadays more commonly used as a valuable validation test for the strength models used in hydrocode simulations. For this purpose, adding time-resolved data of the deformation (e.g. high-speed imaging) provides additional constraints and therefore offers the possibility to more finely discern between models. Variations on the traditional Taylor test can deliver other useful data/conditions. Symmetric impact tests [3] allow the removal of friction considerations at the boundary and provide velocimetry diagnostic access to the rear of the target rod. Another option is the use of the reverse impact configuration [4] whereby an 'anvil' is fired at a stationary rod. This test allows the Taylor specimen itself to be tested at initial elevated temperatures in a more controlled manner than if pre-heating the fired rods as required in the traditional or symmetric configurations. It is noted that for the reverse configuration one must accept friction effects at the impact face and note that a fired 'anvil' cannot generally be approximated as infinite, requiring the anvil and any backing material to be explicitly modelled.

In the current experiments we present a series of reverse impact Taylor tests on pure tantalum (Ta) using a bespoke infrared (IR) oven to elevate the sample temperatures up to ~1000 K. The data is compared to Lagrangian hydrocode simulations utilizing three different strength models: Steinberg-Guinan (SG) [5], Preston-Tonks-Wallace (PTW) [6] and the LMS13 multiscale model [7].

EXPERIMENTS

A series of 8 reverse impact Taylor tests were undertaken on pure polycrystalline Ta, exploring the dynamic strength and deformation behaviour at impact velocities ranging between 112 – 185 m/s and with initial sample temperatures between 293 K – 954 K. Cylinders of Ta with nominal length and diameter of 38.1 mm and 7.62 mm

Shock Compression of Condensed Matter - 2022
AIP Conf. Proc. 2844, 260012-1–260012-6; https://doi.org/10.1063/12.0020430
Published by AIP Publishing. 978-0-7354-4225-2/$30.00

respectively were impacted under vacuum by 6 mm thick, 22.5 mm diameter maraging C300 steel flyers (in an as-received unaged condition; yield strength ~ 760 MPa). Flyers were mounted on polycarbonate sabots and launched by means of a 25 mm bore, single stage gas gun located at the Impact and Shock Mechanics Laboratory (ISML) at the University of Oxford. The pure tantalum material used in these experiments was of the same stock as recently described by Prime *et al.* [8]. The material, with moderately low levels of interstitial impurities, was carefully prepared to produce a relatively uniform microstructure and was provided in the form of 10 mm thick plate stock. Due to the Taylor specimen dimensions, samples were necessarily cut to orient the loading axis perpendicular to the plate thickness direction.

Images of the experimental setup are given in Fig. 1. The rod was suspended along the axis of the barrel using two pairs of thin wires (one pair looped from above, one from below). Initial experiments used 50 µm invar wire to minimize thermal expansion and maintain alignment although this was replaced in the later experiments by 125 µm thermocouple wires to improve specimen temperature measurements up to the point of impact. Fine rod alignment was achieved through laser alignment and kinematic mounts attached to the wires above and below the furnace. To reduce alignment issues due to thermal expansion as the sample was heated, the wires were attached to the kinematic mounts through small pretensioned springs (at a few tens of N). The thermocouples were insulated from the springs with glass-ceramic washers and rollers.

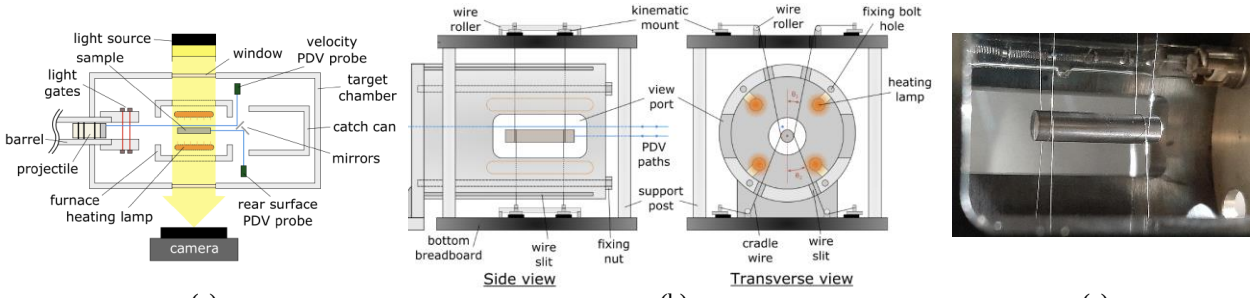

FIGURE 1. Images of the experimental set-up. (a) Schematic illustration of the optical relay and probe paths. (b) Illustration of experimental set-up showing heating lamps and sample mounting system. (c) Photograph of suspended Taylor specimen through furnace view port.

The velocity measurements from the sample rear surface and the incoming flyer (for most experiments) were provided by means of PDV [9]. The PDV provides the precise impact velocity and timing required for effective comparison to modelling. The PDV were aligned from outside the furnace via mirrors with alignment to the rod centre estimated to be within ± 1 mm. The rear surface of the rods were hand polished to produce a near diffuse surface for the PDV measurements. The sample was protected from any possible oxidation by cyclically purging the impact chamber with argon prior to pulling the final experimental vacuum and heating the rod.

High-speed photography was performed during the Taylor impact tests to capture multiple frames of the transient deformation profile of the specimen. Samples were back lit with 1-2 kW flash lighting and images were captured using either a Shimadzu HPV-X2 high speed video camera or a Specialised Imaging SIMX-16 high speed framing camera. A pair of light gates positioned at the muzzle of the barrel were used to measure approximate impact velocity and trigger subsequent diagnostics such as the flash and camera for high-speed imaging, and the PDV. A third light-gate was introduced nearer to the front of the target rod in some experiments to provide a more precise trigger for the framing camera used. Soft recovery of the impacted Taylor specimen was not attempted due to the proximity of down range diagnostics such as the PDV probes and mirrors. Whilst recovered specimens have been scanned and metrologised, the significant post impact deformation means that limited emphasis is placed on this data.

RESULTS

Example results are shown in the following figures. Figure 2 shows rear surface PDV velocimetry for the experiments highlighting the effects of impact velocity and temperature. Figure 3 shows a series of high-speed imaging frames for two experiments fired at ~ 180 m/s at 660 K and 807 K respectively.

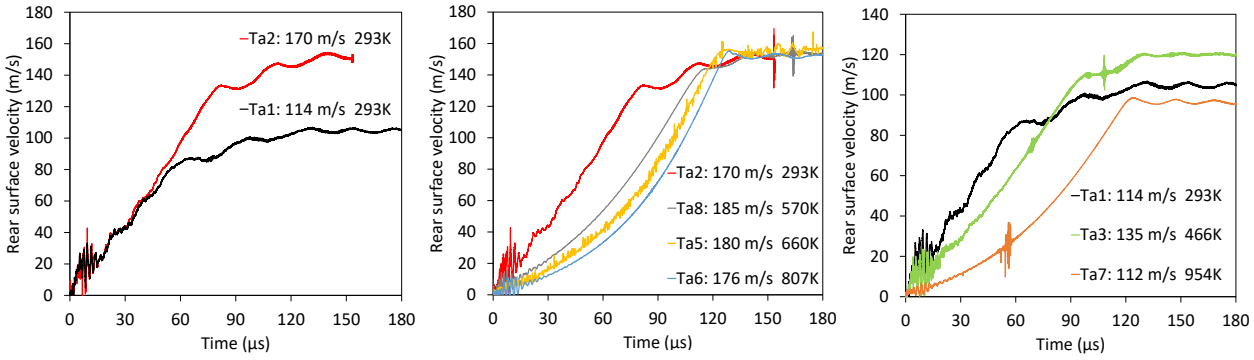

(a) (b) (c)

FIGURE 2. Rear surface velocimetry data for (a) samples tested at room temperature with two impact velocities, (b) samples tested at an impact velocity ~ 180 m/s at different initial temperatures and (c) samples tested at lower impact velocities across the full range of temperature.

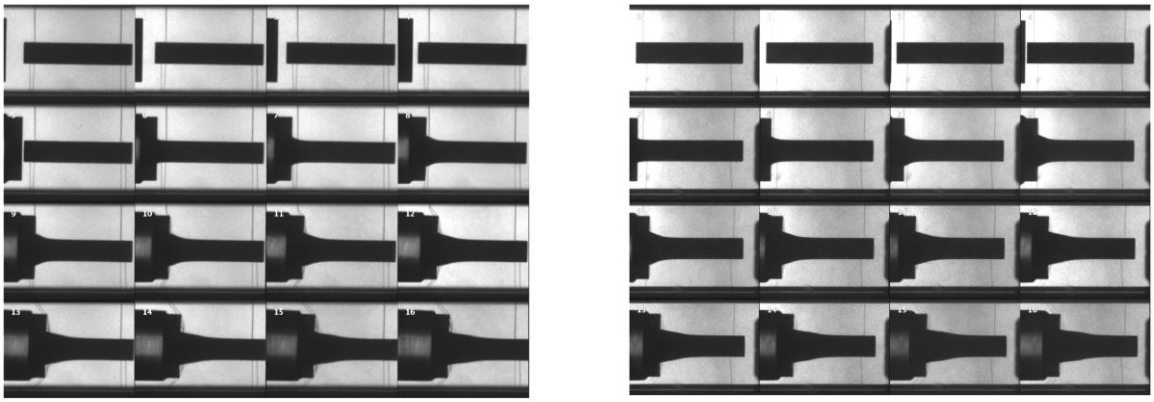

(a) Shot 5: 180 m/s, 660 K (b) Shot 6: 176 m/s, 807 K

FIGURE 3. High-speed framing camera data (SIMX-16) for comparable impact velocity shots at two different initial sample temperatures. Interframe times: 7 μs, exposure times: 0.25 μs, pixels: 1280 x 960 each frame.

In the data displayed in Fig.2 small oscillations are observed in most of the early time (0-20 μs) data originating from radial elastic reverberations within the rod, which are most pronounced when the PDV is centrally focused [10]. Longer time scale features in the form of an initial velocity jump (Δu_{fs}) and a stepped loading profile (~16 μs spaced steps) can be seen in the room temperature and 466 K data sets. The initial velocity jump is due to the initial yield strength, which can be simply approximated as σ_y ~ 500 MPa at room temperature and ~ 347 MPa at 466 K, using $\frac{1}{2}\rho c \Delta u_{fs}$, where ρ is density and c is the slender rod approximation for elastic wave velocity calculated from Young's modulus E as $c=(E/\rho)^{1/2}$ [11]. The stepped profile is then due to the reverberation of this elastic behaviour from the rear surface and off the much slower oncoming plastic wave (which is the part which causes the lateral motion of material at the impact end). At higher initial temperatures the yield and stepped features reduce (Fig.2(b)), disappear (Fig.2 (b) and (c)) and the velocities become a smooth concave curve. At the lower temperature end the velocity profiles reach the turning point towards the plateau velocity at an earlier time, although the ultimate plateau velocities are independent of initial temperature. In Fig.2(a) it is also observed that the initial ramp for the same temperature experiments is largely independent of impact velocity. In Fig.2 (b) and (c) there is an apparent reduction in amplitude of the radial oscillations with temperature. As increasing the rod temperature led to more challenges in maintaining PDV alignment this could be real but may also be affected by any movement of the PDV spot further from the centre of the rod.

SIMULATIONS AND DISCUSSION

A series of 2D Lagrangian finite element hydrocode simulations have been undertaken to study the data in this research utilizing a SG strength model [5, 12], a PTW strength model [6] parameterised at AWE using mainly high rate SHPB data and quasi-static loading data at varied temperature [13] and the multiscale LMS13 [7] strength model. Comparisons between mid-deformation high-speed camera data and simulations are presented in Fig.4(a) for Shots 4 – 6 at impact velocities ~ 175 m/s and three temperatures between 562 K and 807 K. Figure 4(b) shows an example post-shot 3D scan of a recovered rod and anvil showing a noticeable indent in the flyer of ~ 0.3 mm depth and corresponding bulge on the rod face which are generally matched well in the simulations using LMS13 and PTW as shown in Fig.4(a). Post-test impact damage is also noticeable in the image in Fig.4(b).

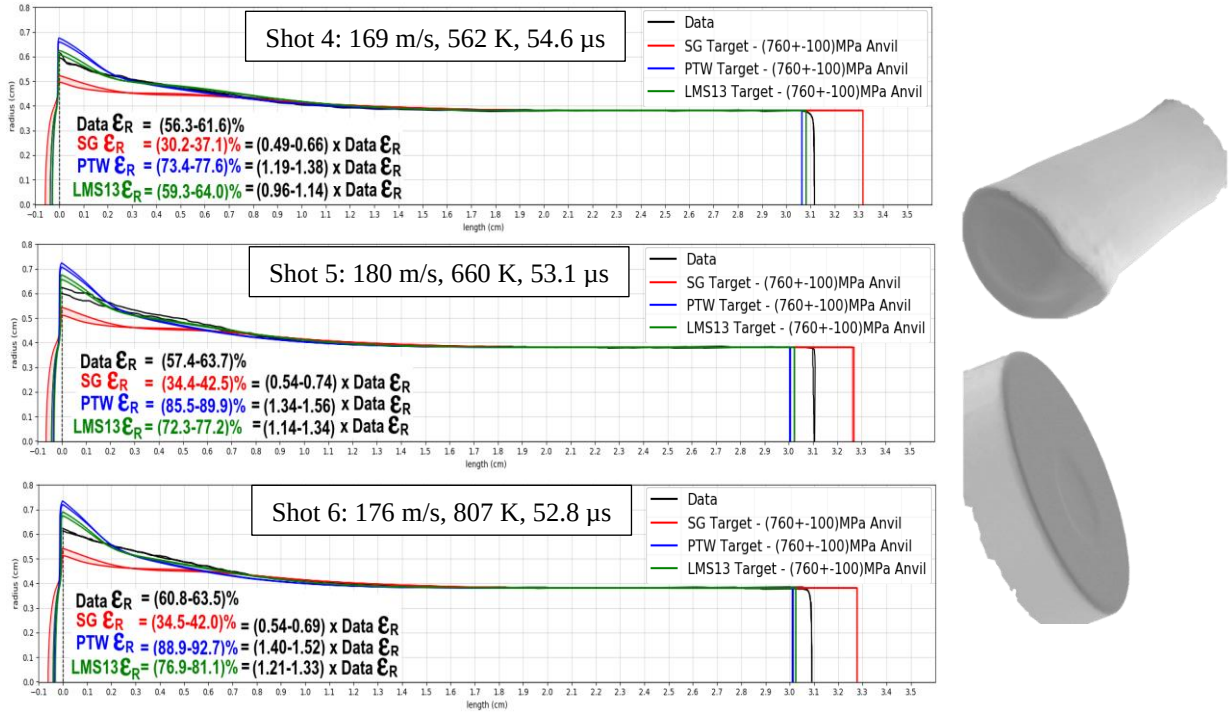

FIGURE 4. (a) Plots of high-speed camera versus simulated data for Shots 4 – 6. The two data curves for each represent the top and bottom of the rod respectively. The two curves for each simulated profile represent the results due to the estimated uncertainty in the yield strength of the steel anvil. (b) Example 3D scan of recovered sample and anvil.

From Fig.4(a) it is seen that the multiscale LMS13 model matches the data most accurately although radial strains become increasingly dissimilar with increasing temperature as the front ~ 0.2 cm expands more significantly in the simulations. Longitudinal strain is also better matched at 562K down to room temperatures (not shown) for LMS13 as well as PTW although it is not clear how the fit quality varies with temperature. Overall, in comparison to the data, PTW is presenting as too weak whilst SG is too strong.

Example simulated velocimetry traces from Shot 1 (114 m/s, 293 K) and Shot 7 (112 m/s, 954 K) are compared to the recorded data in Fig.5(a). As can be seen in Shot 1, SG generally overpredicts the surface velocity although the first 10-25 µs are matched reasonably well by SG as well as PTW and LMS13. From 25-50 µs SG and the data show the stepped structure discussed previously but this structure is missed by PTW and LMS13. For Shot 7 SG performs poorly, overpredicting the velocity across the full experimental time and continuing to predict the stepped structure which is now absent at high temperatures in the data. Modification of the tantalum strength in the SG model leads to a smoothing out of the stepped features as shown in Fig.5(b). Calibration of this strength allows a closer match to the slope of the data and the other models (Fig.5(c)), however the detailed structure is not fully captured.

The simulated matches to the full data sets (rod shape and velocimetry) are most accurate for the LMS13 model, however the match is imperfect in some regard for all three models. This highlights a key benefit of these experiments as imposing the constraint of different data sets allows for more robust improvement and validation of strength models.

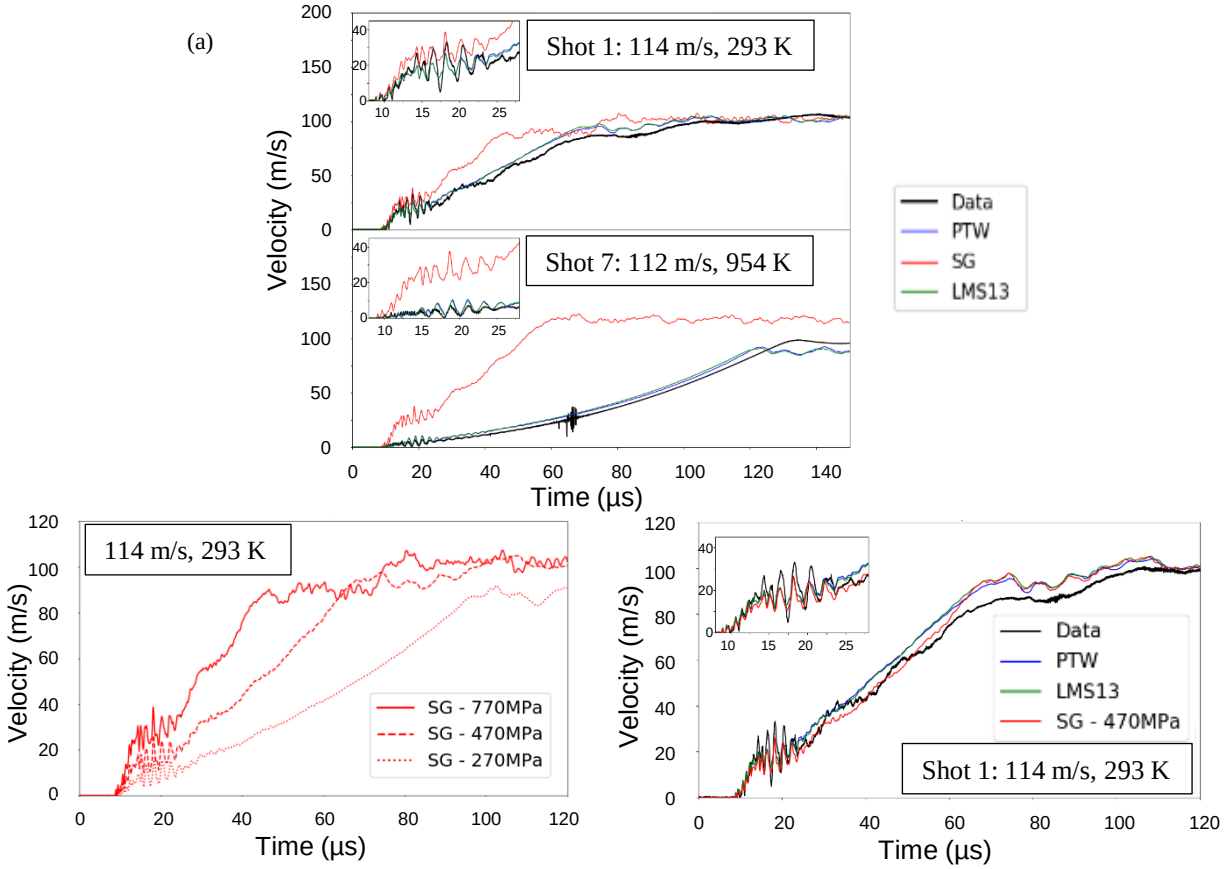

FIGURE 5. Comparisons of rear surface velocimetry data with various strength models. (a) Plots of velocimetry for Shots 1 and 7 compared to SG, PTW and LMS13 models. (b) Simulated velocimetry for Shot 1 using the SG model altering yield strength. (c) Comparison of data to all three models using SG model calibrated to match slope of data.

CONCLUSION & FURTHER WORK

In this paper we have presented a series of heated reverse Taylor impact experiments using a bespoke IR oven and thermocouple wire cradle method to suspend rods of Ta whilst time-resolved deformation was recorded by means of high-speed imaging and rear surface velocimetry. Simulations have been performed to compare with experimental data with impact velocities ranging between 112 – 185 m/s and with initial sample temperatures between 293K – 954K. With the current parameterisation it appears that SG overpredicts Ta strength, PTW underpredicts Ta strength and LMS13 is similarly accurate to PTW in capturing rear surface velocity data but appears to better capture the forms recorded on high-speed imaging. The accuracy of models' temperature sensitivity is however not yet clear. Further study of the recovered rods and high-speed imaging will soon be undertaken to assess any potential ovality of the rod deformation and the effects of any tilt in the impacts.

ACKNOWLEDGMENTS

The authors would like to graciously acknowledge Nathan Barton of LLNL for the provision of the tantalum material used in this research and Emilio Escauriza for his assistance with the experiments. UK Ministry of Defence © Crown Owned Copyright 2022/AWE.

REFERENCES

1. G. I. Taylor, Proceedings of the Royal Society of London. Series A. Mathematical and Physical Sciences **194** (1038), 289-299 (1948).
2. A. C. Whiffin and G. I. Taylor, Proceedings of the Royal Society of London. Series A. Mathematical and Physical Sciences **194** (1038), 300-322 (1948).
3. D. C. Erlich, D. A. Shockey and L. Seaman, AIP Conference Proceedings **78** (1), 402-406 (1982).
4. W. H. Gust, Journal of Applied Physics **53** (5), 3566-3575 (1982).
5. D. J. Steinberg, S. G. Cochran and M. W. Guinan, Journal of Applied Physics **51** (3), 1498-1504 (1980).
6. D. L. Preston, D. L. Tonks and D. C. Wallace, Journal of Applied Physics **93** (1), 211-220 (2002).
7. N. R. Barton and M. Rhee, J. App. Phys **114**, 123507 (2013).
8. M. B. Prime, A. Arsenlis, R. A. Austin, N. R. Barton, C. C. Battaile, J. L. Brown, L. Burakovsky, W. T. Buttler, S.-R. Chen, D. M. Dattelbaum, S. J. Fensin, D. G. Flicker, G. T. Gray, C. Greeff, D. R. Jones, J. M. D. Lane, H. Lim, D. J. Luscher, T. R. Mattsson, J. M. McNaney, H.-S. Park, P. D. Powell, S. T. Prisbrey, B. A. Remington, R. E. Rudd, S. K. Sjue and D. C. Swift, Acta Materialia **231**, 117875 (2022).
9. O. T. Strand, Rev. Sci. Instrum. **77**, 083018 (2006).
10. D. E. Eakins and N. N. Thadhani, Journal of Applied Physics **100** (7), 073503 (2006).
11. I. Rohr, H. Nahme and K. Thoma, J. Phys. IV France **110**, 513-518 (2003).
12. D. J. Steinberg, UCRL-MA-106439 (LLNL) (1991).
13. S. R. Chen and G. T. Gray, Metallurgical and Materials Transactions A **27** (10), 2994-3006 (1996).